Journal of Magnetism and Magnetic Materials 460 (2018) 320–326

Contents lists available at ScienceDirect

Journal of Magnetism and Magnetic Materials

journal homepage: www.elsevier.com/locate/jmmm

Research articles

Strange non-chaotic attractors in spin valve systems

A.M. Cabanas [a,*], L.M. Pérez [b], D. Laroze [a,b]

[a] Instituto de Alta Investigación, Universidad de Tarapacá, Casilla 7D, Arica, Chile
[b] School of Physical Sciences and Nanotechnology, Yachay Tech University, 00119 Urcuquí, Ecuador

ARTICLE INFO

Article history:
Received 6 November 2017
Received in revised form 16 February 2018
Accepted 11 April 2018
Available online 12 April 2018

Keywords:
Magnetization dynamics
Strange non-chaotic attractors
Chaos

ABSTRACT

The current-driven magnetization dynamics in spin torque oscillators is investigated because of its high potential for high-frequency applications. The system consists of a pinned layer with a fixed magnetization and a single-domain free layer, such that it is governed by the Landau-Lifshitz-Gilbert-Slonczewski equation. In particular, we study the effect of a time-dependent quasi-periodic current. We numerically characterize the dynamical behavior of the system by monitoring the Lyapunov exponents, and by calculating the Fourier spectra. We find a rather complicated landscape of sometimes closely intermingled chaotic and non-chaotic areas in the parameters space. Finally, we compute a phase diagram of the existence of the strange non-chaotic attractors.

© 2018 Elsevier B.V. All rights reserved.

1. Introduction

Quasi-periodic driven nonlinear systems have been studied in the last decades since new types of dynamical behavior can be found. Indeed, apart from regular and chaotic states a new class of dynamical states called *strange nonchaotic attractors* (SNAs) have been reported [1–8]. These states are characterized by the facts that they do not have sensitive dependence on the initial conditions (non-positive largest Lyapunov exponent) [1] and their corresponding attractors have fractal structures [9,10]. In addition, the spectral function of the Fourier spectrum for the SNAs obeys an inverse power-law scaling relationship [11,12]. These states have been experimentally observed in different two-frequency driven systems. In particular, in quasi-periodically driven magnetoelastic ribbons [11], in neon glow discharge [13], in the movement of stars [14] and driven nonlinear electric circuits [12,15–18], just to mention a few. Respect to theoretical models, SNAs have been studied in discrete maps [1,8,4,19–21] as well as in ordinary differential equations [2,4,12,6,22]. In the last case, the driving can be a direct or a parametric one.

In the framework of parametrically driven systems, classical magnetic systems represent a genuine physical prototype, since the corresponding equations of motion contain torques that are produced by the cross product of the magnetization with a different kind of effective fields [23]. Quasi-periodicity, bi-stability and chaos have been found in simple magnetic systems under an external time-dependent magnetic field [24–29]. Furthermore, other types of dynamical states can appear when the electrical current is taken into account. The proposal of spin-polarized current-induced magnetization dynamics of Slonczewski [30] and Berger [31] initiated a huge amount of theoretical and experimental studies in the last decade. This new phenomenon has important applications in spintronics [32].

The use of spin current is a key for the technological development of high-frequency current-tuneable nanoscale oscillators, like magnetic random access memory (MRAM) [33,34]. For MRAM applications, the spin-transfer effect is responsible for the magnetization reversion of a bit. When a large magnetic field is applied, the spin-transfer torque can induce uniform precession of the free layer magnetization about the axis of the applied field. Due to the coupling with the giant magnetoresistance effect (GMR) [35,36], this precession produces a voltage response that makes these devices high-frequency oscillators.

Theoretical models and their different aspects can be found in the literature, and the state-of-the-art is given in the Refs. [37,38]. Chaotic regimes in spin valves were predicted by Li et al. [39,40]. Other subsequent works about chaos in magnetic systems with spin torque effect and different configurations of the magnetic field and electric current can be found in Refs. [41–52]. Besides, recent experiments about stationary states, precessional states and nonlinear behaviors in these systems were performed by Kiselev et al. [53,54], by Krivorotov et al. [55] and by Nagasawa et al. [56].

The aim of this paper is to study the effect of quasi-periodic electrical current in a spin valve oscillator. The single-domain free layer is governed by the Landau-Lifshitz-Gilbert-Slonzewski system in the presence of a static magnetic field and a time-dependent

* Corresponding author.
E-mail address: ana.cabanas.plana@gmail.com (A.M. Cabanas).

https://doi.org/10.1016/j.jmmm.2018.04.024
0304-8853/© 2018 Elsevier B.V. All rights reserved.

applied current. The magnetization dynamics of free layer is deeply investigated with different dynamical indicators as a function of the parameters. The manuscript is organized as follows: In Section 2 the theoretical model is presented. In Section 3 the results obtained by the numerical simulations are analyzed. Finally, the conclusions are exposed in Section 4.

2. Theoretical model

Let us consider a spin-valve device under the effect of an electrical current, J_e, and an external magnetic field $\mathbf{h}$. This device is known as a nano-pillar structure and has at least two ferromagnetic layers with about 100 nm in lateral size separated by a non-magnetic material layer, usually called spacer. In the range of film thicknesses most commonly used, the spin valve model consists of a pinned layer with a fixed magnetization at a specific direction $\mathbf{M_f}$ and a single-domain free layer, with a magnetization vector $\mathbf{M}$. The pinned layer has a large magnetocrystalline anisotropy, or it is thicker than the free layer acting as a polarizer for the electric current. The dynamics of $\mathbf{M}$ is determined by the Landau-Lifshitz-Gil bert-Slonzewski (LLGS) equation [39,40]:

$$\frac{d\mathbf{m}}{dt} = -\mathbf{m}\times\Gamma + \eta\mathbf{m}\times\frac{d\mathbf{m}}{dt} + g\mathbf{m}\times(\mathbf{m}\times\hat{\mathbf{p}}) \tag{1}$$

where $\mathbf{m} = \mathbf{M}/M_s$, $t = T|\gamma|M_s$ [23], and $\hat{\mathbf{p}} = \mathbf{m_f}$. Here M_s is the saturation magnetization that leads to $|\mathbf{m}| = 1$ and γ is the gyromagnetic factor associated with the electron spin with a numerical value approximately given by $|\gamma| = |\gamma_e|\mu_0 \approx 2.21\times10^5$ m A^{-1} s^{-1}. To get a better physical insight into the problem, we evaluate the scales introduced here. Typical values are, e.g. for cobalt materials, $M_s \approx 1.42\times10^6$ A/m ≈ 17.8 kOe [39,40,54], hence the time scale ($T = 1$) is in the picosecond range $t_c = 1/(|\gamma|M_s) \approx 3.2$ ps [23]. Let us remark that a characteristic frequency of the system is $\omega_c = |\gamma|M_s/(2\pi) = 49.95$ GHz. Besides, there have been reported some experiments that observe the spin dynamics at 100 ps [53,43,60] and also below the picosecond scale [57]. In fact, the present technology is able to work at time scale less than 100 fs [58,59].

In the above equation, η denotes the dimensionless phenomenological damping coefficient characteristic for this material, in the case of cobalt $\eta(Co) \sim 10^{-2}$ [23,61]. In Eq. (1), the effective field denoted by Γ has contributions of an external field, anisotropy, and a demagnetization field perpendicular to the layer (z-axis). Therefore, it can be written as

$$\Gamma = \mathbf{h} + \beta_x(\mathbf{m}\cdot\hat{\mathbf{x}})\hat{\mathbf{x}} - \beta_z(\mathbf{m}\cdot\hat{\mathbf{z}})\hat{\mathbf{z}}, \tag{2}$$

where $\mathbf{h} = \mathbf{H}/M_s$ is the external magnetic field, β_x and β_z are the dimensionless anisotropy constants for the x-axis (easy axis) and the z-axis (hard axis), respectively. They are combinations of the normalized anisotropy and the demagnetization constants with respect to these axes. This special type of anisotropy is called biaxial anisotropy. The anisotropy constants can be positive or negative depending on the specific substance in use [62]. In our case both coefficients are positive, so β_x will favor the free magnetization in the x-axis while β_z will disfavor it. On the other hand, for sub-nanometer thick cobalt, the magnetization points perpendicular to the plane as a result of the interface anisotropy as it is shown in Ref. [63]. Thus, the perpendicular-to-plane anisotropy coefficient β_z can be controlled by the layer thickness. In particular, we fix $\beta_x = 1/2$ and $\beta_z = 1$. We also assume that the external field is constant in the $\hat{\mathbf{x}}$ direction, $\mathbf{h} = h_x\hat{\mathbf{x}}$. Since the field is normalized by M_s, the order of magnitude is in the range of 10^1 kOe. Thus we will vary h_x in this range.

The term $g\mathbf{m}\times(\mathbf{m}\times\hat{\mathbf{p}})$ in Eq. (1) accounts for spin transfer where g is the amplitude of the spin transfer torque proportional to the spin-polarized current density; and $\hat{\mathbf{p}}$ is the unit vector associated with the fixed layer of the spin-valve. Indeed, $g = \mathcal{F}(\mathbf{m})J_e\mathcal{P}\hbar/(2|e|\mu_0 dM_s^2)$ [52] where $\mathcal{P}$ is the spin polarization of the current, typical values $\mathcal{P}(Co) \approx 0.35$ [30,23], μ_0 is the magnetic permeability of free space, e is the electric charge, d is the thickness of the free layer and $\mathcal{F}(\mathbf{m})$ is a model-dependent function [39,40,47,23]. For the sake of simplicity, the analysis is limited to consider $\mathcal{F}(\mathbf{m}) \approx 1$ [39,40,47]. This is known as the sine-approximation [64,61,65,52,66], and it is commonly adopted for certain types of nanopillars [67,68]. In what follows, we will assume that $\hat{\mathbf{p}} = \hat{\mathbf{x}}$. $J_e = J_e(t)$ denotes the time-dependent current density described by a two-frequency modulation that flows in the x-direction, experimental values range $J_e \approx 10^7 - 10^9$ A/cm^2 [53,54,52,69–73]. The threshold current density required for switching the magnetization is $J_p = (|e|\mu_0 dM_s^2)/\hbar$ [23,41,34], for a 3 nm thick layer of cobalt $J_p \approx 1.1\times10^9$ A/cm^2. Hence, the function g(t) can be cast in the form:

$$g(t) = g_0 + g_1\cos(\omega_1 t) + g_2\cos(\omega_2 t), \tag{3}$$

where $\{g_0, g_1, \omega_1, g_2, \omega_2\}$ are time-independent coefficients. g_0 is the continuous part of the current and the parameters g_1 and g_2 correspond to the time dependent current. Since $J_p \approx 1.1\times10^9$ A/cm^2 and $J_e \approx 10^7 - 10^9$ A/cm^2 implies a value of $g_i \approx 10^{-3} - 10^1$ [23]. In the present study we will analyze the amplitude of the current in this range. In addition, notice that the frequencies are normalized by $|\gamma|M_s$, which in the case of cobalt has a value of 314 s^{-1} [23].

Notice, that there are two relevant cases for the ratio of the frequencies ω_1/ω_2. When ω_1/ω_2 is rational, the system is periodically forced, whereas an irrational quotient produces a quasi-periodic forcing. In the following, we will study the behavior of the system as a function of these control parameters for a quasi-periodic modulation.

Let us first write Eq. (1) in a practical form. For this purpose we define $\Gamma_{est} = \Gamma - g(t)\mathbf{m}\times\hat{\mathbf{x}}$, replacing this definition, Eq. (1) has the same structure as the Landau-Lifshitz-Gilbert equation, which means that

$$\frac{d\mathbf{m}}{dt} = -\mathbf{m}\times\mathbf{\Gamma}_{est} + \eta\mathbf{m}\times\frac{d\mathbf{m}}{dt}, \tag{4}$$

and therefore, Eq. (4) can be written as [24]:

$$\frac{d\mathbf{m}}{d\tau} = -\mathbf{m}\times\mathbf{\Gamma}_{est} - \eta\mathbf{m}\times(\mathbf{m}\times\Gamma_{est}), \tag{5}$$

where $\tau = t/\kappa$ with $\kappa = 1+\eta^2$, and consequently the frequency is normalized as $\Omega_i = \kappa\omega_i$. Notice that the factor κ has a small contribution, for instance in the case of cobalt materials one has $\kappa \approx 1.0001$ and $1/\kappa \approx 0.9999$.

Let us comment that when the system has only a constant current one can analytically calculate its natural frequency. Taken into account that the magnitude of the magnetization is a constant ($|\mathbf{m}| = 1$) and assuming that $m_y^2 \sim m_z^2 << 1$, the LLGS equation can be linearized and expressed in terms of one independent variable as [50]:

$$\frac{d^2m_y}{dt^2} = -\bar{\omega}_0^2 m_y - \bar{\mu}\frac{dm_y}{dt}, \tag{6}$$

where $\bar{\omega}_0^2 = (1+\alpha^2)\left[(h_0+\beta_x)(\beta_z+h_0+\beta_x)+g_0^2\right]$ and $\bar{\mu} = (\alpha(\beta_z/2 + h_0+\beta_x) - g_0)/2$. This is the equation of a damped harmonic oscillator such that $\bar{\omega}_0$ and $\bar{\mu}$ are the natural frequency and the dissipation coefficient, respectively. In the next section, we will present the numerical results obtained from the simulations.

3. Simulations

This section is divided into two parts. In the first subsection, the quantities that are commonly used to describe different dynamic states are presented. In the second subsection numerical simulations are performed and analyzed, in order to identify different kinds of dynamical behaviors.

3.1. Dynamical indicators

A hallmark of chaotic dynamical behavior is the exponential separation of the nearby trajectories in time. Lyapunov exponents describe the rate of exponential divergence from perturbed initial conditions [76,74,75] and serve as a useful tool to quantify chaos. We characterize the dynamics of Eq. (5) by evaluating the largest Lyapunov exponents (λ_{max}) given by:

$$\lambda_{\max} = \lim_{\tau\to\infty}\left[\frac{1}{\tau}\ln\left(\frac{|\delta\mathbf{m}(\tau)|}{|\delta\mathbf{m}(\tau_0)|}\right)\right], \tag{7}$$

where $\delta\mathbf{m}$ satisfies the linear differential equation:

$$\frac{\partial\delta\mathbf{m}}{\partial\tau} = \bar{\mathbf{J}}\cdot\delta\mathbf{m}, \tag{8}$$

where $\bar{\mathbf{J}}$ is the Jacobian matrix of the system, which is, in general, a function of the magnetization i.e. $\bar{\mathbf{J}} = \bar{\mathbf{J}}[\mathbf{m}]$. Note that two magnetic configurations that were infinitesimally close at $\tau = \tau_0$, separate in phase space exponentially fast when the system is chaotic, $\lambda_{\max} > 0$. On the other hand, for a negative largest Lyapunov exponent ($\lambda_{\max} < 0$), the two initially close states converge to the same attractor. The marginal case $\lambda_{\max} = 0$ corresponds to solutions whose orbits are time-periodic or quasi-periodic. Moreover, because the system is driven by a two-frequency time-dependent current, strange non-chaotic attractor [1,4,8] might appear [22,2,77]. The SNAs have non-positive λ_{max}. Therefore nearby orbits do not diverge exponentially in time. A strange non-chaotic attractor is an attractor which is neither a finite set of points nor is it piecewise differentiable [77]. The word strange refers to the geometrical fractal structure of the attractor [9]. A significant feature of SNAs is that they appear to be typical in quasi-periodically forced systems as quasi-periodically forced damped pendula [77], quantum particles in quasi-periodic potentials [2], and in biological oscillators [78,79] in which different mechanisms have been proposed. Although these attractors can suddenly appear as the parameters of the system are changed [1], the route by which they emerge is still an interesting question.

In this paper, we focus on the formation of the SNAs as the parameters are changed. For instance, one can draw two-dimensional maps illustrating the magnitude of λ_{max} as a function of two parameters. This allows us to determine the parameter ranges that lead to chaotic behaviors, i.e. λ_{max} positive, and those showing quasi-periodic, periodic or SNAs states with negative or zero λ_{max}. Additionally, following a technique explained in Ref. [80,81], we use an iterative zoom resolution process to further investigate the dependence of the dynamics upon minimal variations of the system parameters.

Let us also comment that other complementary methods should be applied to discriminate between nonchaotic states such as the Fourier spectrum, Poincaré sections, correlation functions, Melnikov functions, etc [39,40,43,47,25,82–88]. The classical one is the Fourier spectrum, which we denote by $S(f)$. Using this spectrum, one can define the spectral distribution function $N(\sigma)$ as the number of peaks of $|S(f)|$ with an amplitude greater than σ. This quantity obeys different scaling laws depending on the dynamical behavior. In particular, $N(\sigma) \propto \ln(1/\sigma)$ for a two-frequency quasi-periodic attractor, $N(\sigma) \propto \ln^2(1/\sigma)$ for a three-frequency quasi-periodic attractor, and $N(\sigma) \propto \sigma^{-\alpha}$, with $1 < \alpha < 2$, for strange non-chaotic attractors [2,11]. Therefore, we will explore the dependence of λ_{max} and $N(\sigma)$ on the different control parameters to characterize our system.

3.2. Numerical results

In order to integrate the equation of motion and avoid numerical artefacts, it is convenient to solve Eq. (5) in the Cartesian representation by using a standard fourth order Runge–Kutta integration scheme with a fixed time step $d\tau = 0.01$ that ensures a precision of 10^{-8} on the magnetization field. Due to the large number of parameters involved in the system, we first set $\eta = 0.05$, $\beta_x = 0.5$, $\beta_z = 1.0$, $h_x = 1.0$, $\Omega_1 = 1.0$, $\Omega_2 = \pi/4$ and $g_0 = 0.1$ while g_1 and g_2 are varied.

Since the largest Lyapunov exponent is the standard quantitative criterion to determine the dynamical behavior of a system Fig. 1 shows the color-coded λ_{max} as a function of the current amplitudes g_1 and g_2. These two current amplitudes determine the quasi-periodic modulation. As it is shown by the colorbar, black shadings are used to denote non-chaotic phases ($\lambda_{max} \leqslant 0$) while colors represent the chaotic ones ($\lambda_{max} > 0$). On the left panel, we observe non-chaotic regimes when g_1 and g_2 are close to zero and in the upper region close to $g_2 = 4$. Note that the chaotic region between $g_1 = (2.0, 4.0)$ is not compact, but contains areas of

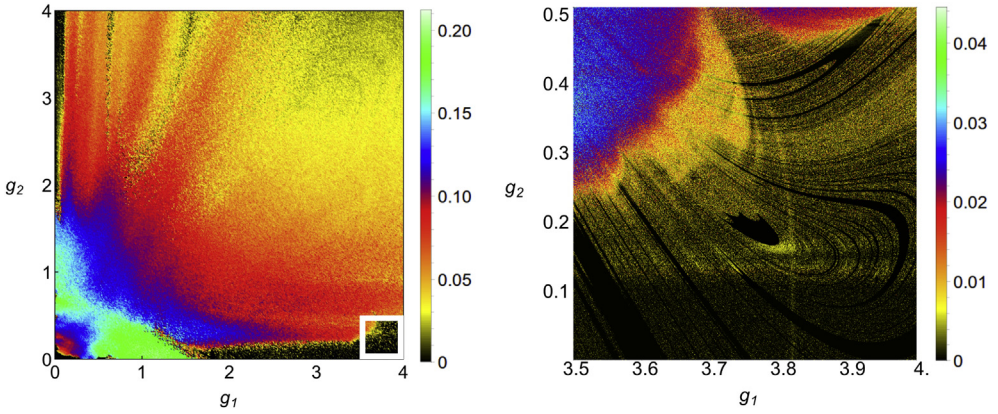


Fig. 1. Phase diagram displaying the largest Lyapunov exponent (λ_{max}) in a color-coded code as a function of the current amplitudes g_1 and g_2 for the fixed parameters $\Omega_1 = 1$, $\Omega_2 = \pi/4$, $h_x = 1$, $g_0 = 0.1$, $\beta_x = 0.5$, $\beta_z = 1$ and $\alpha = 0.05$. The color bars for the λ_{max} range identify the regions of chaotic (colors) and non-chaotic (black) dynamics. The parameter resolutions of the right and left panel are $\Delta g_1 = \Delta g_2 = 2.5 \times 10^{-3}$ and $\Delta g_1 = \Delta g_2 = 5.0 \times 10^{-4}$, respectively. (For interpretation of the references to colour in this figure legend, the reader is referred to the web version of this article.)

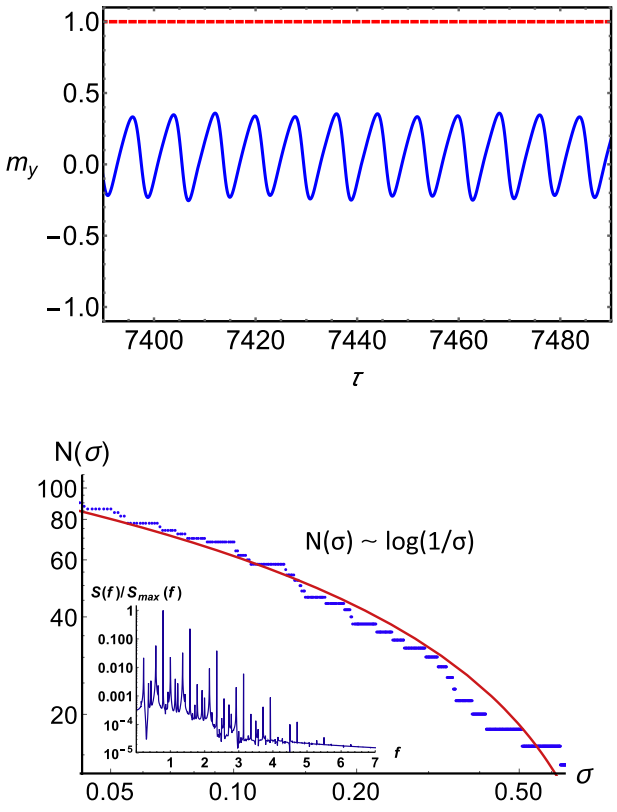


Fig. 2. Upper panel, component m_y (solid blue line) and $|\mathbf{m}|$ (dashed red line) as a function of time for a quasi-periodic state. Lower panel, spectral distribution function $N(\sigma)$ as a function of σ. The inset displays the amplitude of the Fourier transforms. Here, $g_1 = 0.01, g_2 = 0.05$ and $\lambda_{max} = -4.5 \times 10^{-5}$. The fixed parameters are the same of the Fig. 1. (For interpretation of the references to colour in this figure legend, the reader is referred to the web version of this article.)

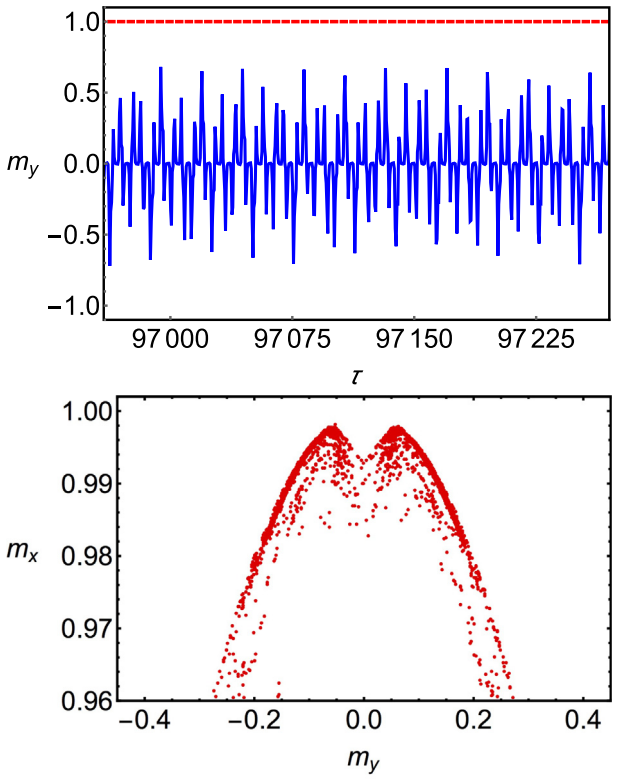


Fig. 3. Upper panel shows the component m_y (solid blue line) and $|\mathbf{m}|$ (dashed red line) as a function of time for a chaotic state. Lower panel displays the 2D Poincaré section of (m_x, m_y) at time interval of $2\pi/\Omega_1$. Notice that here $\lambda_{max} = 0.011$ and $g_1 = 3.80$ and $g_2 = 0.16$. The fixed parameters are the same of the Fig. 1. (For interpretation of the references to colour in this figure legend, the reader is referred to the web version of this article.)

non-chaotic dynamics for specific values of the current amplitude. The right panel is a better resolution of the zoomed-in view of the white square of the left panel and illustrates how chaotic and non-chaotic solutions produce a complex pattern formation in the parameter space. It reveals an interesting footprint-like pattern and a self-similar succession of boomerangs formed by an alternation of phases with different dynamical behaviors [80,81,89–91]. One can recognize that the boundaries separating the regions may be very complicated as they mix continuum branches with diffuse punctual separations.

Furthermore, to investigate in more detail different types of transitions between non-chaotic to chaotic points we analyze several values of the parameter space. For small values of the current amplitudes, $g_1 = 0.01$ and $g_2 = 0.05$, the upper panel of Fig. 2 shows the temporal evolution of the component m_y of the magnetization in a quasi-periodic case. The lower panel displays the spectral distribution function, $N(\sigma)$ as a function of σ. We perform a numerical fit founding that $N(\sigma) = \mu \ln(1/\sigma)$ with $\mu \approx 26.79$, typical for a quasi-periodic behavior. The inset displays the corresponding normalized power spectrum $|S(f)|$. We can identify several dominant frequencies. The value of the λ_{max} is considered as a numerical zero because $\lambda_{max} = -4.5 \times 10^{-5} \approx 0$.

The behavior of the system becomes more complex as the values of the current amplitudes are increased. The top panel of Fig. 3 shows the temporal evolution of the component m_y of the magnetization in a chaotic case with $g_1 = 3.80$ and $g_2 = 0.16$, that is, a point situated next to the right lower corner of the footprint-like shape of the right panel of Fig. 1. The time series of m_y (solid blue line) is not periodic. We estimate a positive value of $\lambda_{max} = 0.011$. The lower panel of Fig. 3 shows 2D Poincaré section of (m_x, m_y) at a time interval of $2\pi/\Omega_1$. Notice that this section is not a regular curve and has several sets of points which is characteristic of a chaotic state.

The temporal evolution of the component m_y for a SNA state (solid blue line) is depicted in the top panel of Fig. 4. The negative largest Lyapunov exponent $\lambda_{max} = -9.28 \times 10^{-4}$ denotes non-chaotic behavior unless the temporal series may appear not regular. The values of the current amplitudes are $g_1 = 3.91$ and $g_2 = 0.42$, thus, regarding the right panel of Fig. 1 this point is enclosed inside the top boomerang. The lower panel of Fig. 4 displays the spectral distribution function, $N(\sigma)$. As in the previous case, we perform a numerical fit founding that $N(\sigma) = \mu\sigma^{-\alpha}$ with $\mu \approx 69.81$ and $\alpha = 1.33$, required condition $(1 < \alpha < 2)$ to find SNAs. The inset displays the corresponding normalized power spectrum $|S(f)|$ represented as a continuum. The corresponding 2D Poincaré section of (m_x, m_y) at a time interval of $2\pi/\Omega_1$ is shown in Fig. 5. It can be observed that this section is a tangled curve. The tangled appearance of these sections is typical for strange attractors. Furthermore, the two insets represent a magnification of the entangled areas where we can distinguish different branches characteristic of multiples loops and roughness.

Based on the analysis of the spectral distribution $N(\sigma)$ for non-positive values of λ_{max} a phase diagram to illustrate the transition from quasi-periodic to SNAs state of the characteristic region of the parameter space shown in the right panel of Fig. 1 is presented in Fig. 6. We find a distribution of SNAs points (red dots) with an inverse power law fit and quasi-periodic states (blue squares) with a logarithmic fit. The light green area corresponds to the chaotic behavior. From the evidence of this numerical results, it is not possible to identify a characteristic pattern for the SNAs distribution in

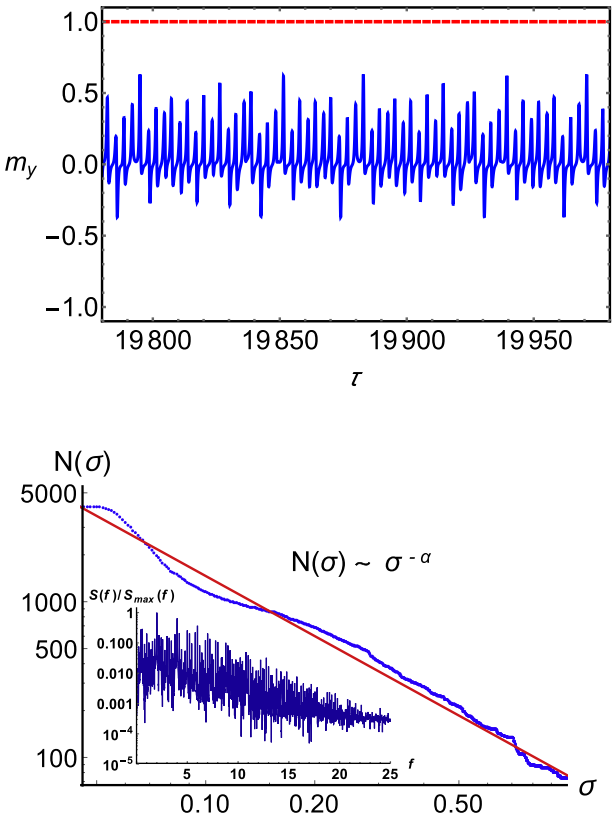


Fig. 4. Top panel shows the component m_y (solid line) and $|\mathbf{m}|$ (dashed line) as a function on time for a SNA state. Lower panel shows the spectral distribution function $N(\sigma)$ with $\alpha = 1.33$. The inset displays the amplitude of the Fourier transform. Here $g_1 = 3.91$, $g_2 = 0.42$ and $\lambda_{max} = -9.28 \times 10^{-4}$. The fixed parameters are the same of the Fig. 1.

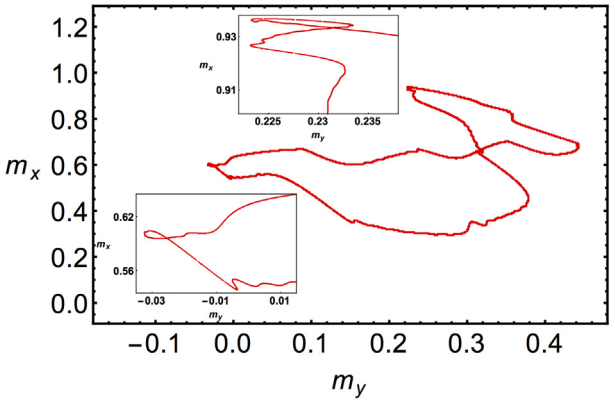


Fig. 5. 2D Poincaré section of (m_x, m_y) at time interval of $2\pi/\Omega_1$ for a SNA state. The two insets correspond to the zoom of two roughness areas depicted. The parameter values are the same of the Fig. 4.

the parameter space in this resolution ($\Delta g_1 = \Delta g_2 = 0.01$). However, we can distinguish a noticeable chaotic sea at the top left corner between $g_1 = (3.50, 3.71)$ and $g_2 = (0.27, 0.50)$.

Apart from the dependence on the quasi-periodic forced current, we study the dependence on the frequency and the magnetic field. The Fig. 7 is a phase diagram of the λ_{max} as a function of g_1 and Ω_1 with $g_2 = 0.2$ and $\Omega_2 = \pi/4$. The scenario changes drastically if we compare with Fig. 1, λ_{max} has now a mirror-inversion symmetry with respect to $\Omega_1 = 0$ with a non-chaotic behavior in its proximity. For values of $g_1 = (2.0, 4.0)$, the system presents non-chaotic

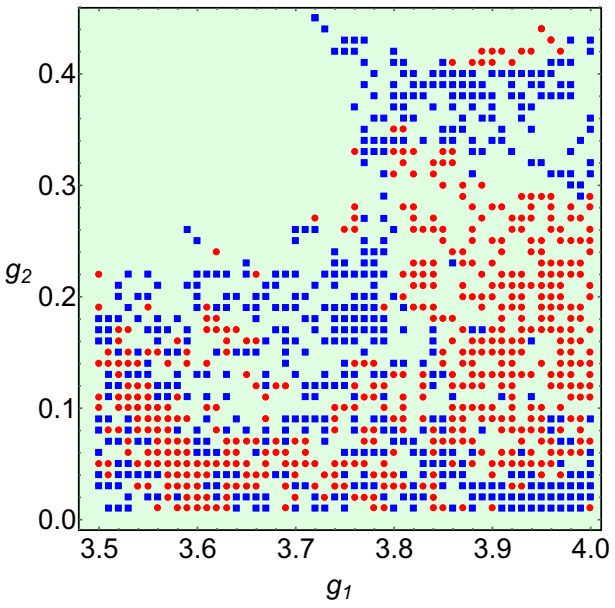


Fig. 6. Phase diagram as a function of g_1 and g_2. The blue squares represent the quasi-periodic states while the red ones represent de SNA points. The fixed parameters are the same of the Fig. 1. (For interpretation of the references to colour in this figure legend, the reader is referred to the web version of this article.)

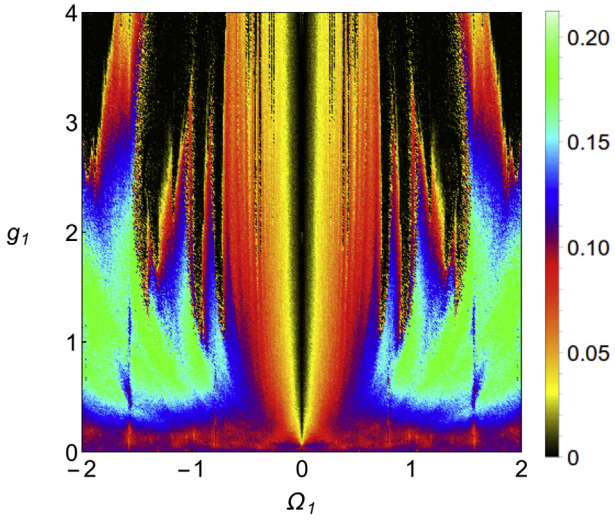


Fig. 7. Phase diagram displaying the largest Lyapunov exponent (λ_{max}) in a color-coded code as a function of the current amplitude g_1 and the frequency Ω_1 at $g_2 = 0.2$. The rest of fixed parameters are the same of the Fig. 1. The parameter resolutions are $\Delta g_1 = \Delta\Omega_1 = 5.0 \times 10^{-4}$. (For interpretation of the references to colour in this figure legend, the reader is referred to the web version of this article.)

states in regions with a spine-like shape while the chaotic areas are concentrated between $g_1 = (0, 2)$ and $\Omega_1 = (|1, 2|)$.

Until now, we have used the following fixed parameters: $h_x = 1$, $g_0 = 0.1$, $\beta_x = 0.5$, $\beta_z = 1$ and $\alpha = 0.05$. If we substitute them in the expression of the natural frequency in the absent of time-dependent currents, $\bar{\omega}_0^2 = (1 + \alpha^2)\left[(h_0 + \beta_x)(\beta_z + h_0 + \beta_x) + g_0^2\right]$, we obtain a value close to $\bar{\omega}_0 \approx 1.94$. Fig. 8 shows λ_{max} as a function of g_1 for near values of $\bar{\omega}_0$. The thick black line corresponds to $\Omega_0 = 1.94$; we observe a transition in the dynamical behavior at $g_1 \approx 2.6$ where the dynamic becomes regular after a period of chaos $\lambda_{max} > 0$. To compare with other values of the driving frequency we vary Ω_i in a close range. We observe that the dynamic is similar in the vicinity, $\Omega_i = \{1.88, 2.0\}$, green and red dashed

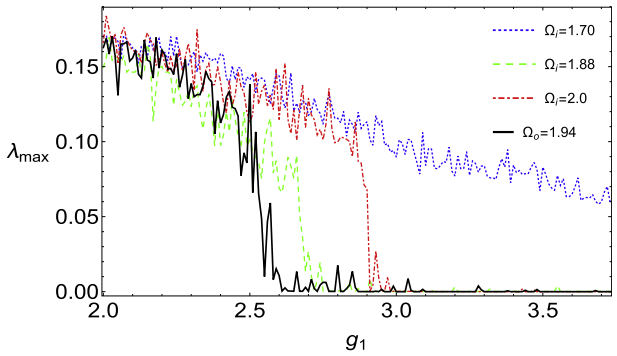


Fig. 8. Largest Lyapunov exponent as a function of g_1 for near values of the natural frequency. The continuum black line corresponds to $\Omega_0 = 1.94$ while the dashed colorful lines are close values. (For interpretation of the references to colour in this figure legend, the reader is referred to the web version of this article.)

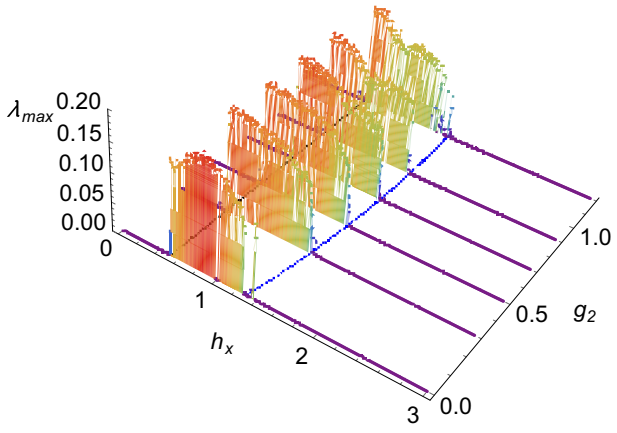


Fig. 9. Largest Lyapunov exponent as a function of h_x and g_2 at $g_1 = 0.5$. The rest of fixed parameters are the same of the Fig. 1. The parameter resolutions are $\Delta h_x = \Delta g_2 = 1.0 \times 10^{-2}$.

lines, respectively. In contrast, for more distant values $\Omega_i = 1.70$ chaos is present for the entire range of g_1.

In order to further study the states distributions due to the changes of the different control parameters, Fig. 9 shows λ_{max} as a function of magnetic field h_x and the current g_2 while $g_1 = 0.5$ is fixed. The transition between regular and chaotic states is clearly visible when λ_{max} jumps from a negative or zero value to a positive one. There is a discontinuous alternation of non-chaotic phases separated by a chaotic area between $h_x \simeq (0.5, 1.4)$ distributed with a similar shape as we increase g_2 from 0 to 1.2. Besides, for $g_2 = 0.0$ we find some non-chaotic points inside of the chaotic region. Furthermore, we can find a linear relationship concerning the first transition among the non-chaotic and the chaotic points such that $h_{x_1}(g_2) = 0.515 - 0.003g_2$ represented as a black dotted line. Likewise, the second transition among the chaotic and non-chaotic states can be fitted by the blue dotted curve, $h_{x_2}(g_2) = -0.24g_2^2 + 0.43g_2 + 1.30$. The regularity of such alternation between chaotic and non-chaotic states allow one to anticipate how big can be the intervals between phases as a function of h_x for a given g_2.

4. Final remarks

The dynamics of the magnetization of a spin valve device under the effect of an external magnetic field **h** and a time-dependent electrical current J_e with a quasi-periodic modulation has been studied in the framework of the LLGS equation. By using two-dimensional maps of the largest Lyapunov exponent in the space parameter, we have examined the effects of minimal variations of the current amplitudes, the frequencies and the external magnetic field, finding that the system is sensitive to these small variations of the control parameters. In fact, we have determined the regions where positive values of this exponent exist and the numerical bounds for the thresholds of the chaotic regimes. By varying the current amplitudes of the quasi-periodic forcing, we find non-chaotic areas at a fixed value of $h_x = 1$ with g_1 and g_2 above zero. We have discovered complex non-chaotic island structures with a footprint-like and boomerang-like shapes, by using a technique of an iterative zoom. Besides, using the spectral function of the Fourier power spectrum, we have found that the system exhibits strange non-chaotic attractors in a wide range of parameters. In particular, we have calculated a phase diagram as a function of the current amplitudes that discriminate the quasi-periodic and the SNAs states based on an inverse power law fit.

The results presented here provide a complementary method through oscillations induced by an alternating spin current with quasiperiodic modulation. The range of the chaotic regime and the SNAs states strongly depends on the values of the time dependent part of the spin-transfer effect g_1 and g_2. Hence, the use of alternating spin-polarized currents opens the possibility to control transitions from regular to chaotic states. These behaviors could open some novel devices functionality to spin-valve devices. To test these SNAs states, we suggest an experimental set-up of spin valves with a size in the range of nanometers, where the monodomain approximation is valid, with a quasi-periodic electrical current under a field in the *kOe* range and frequencies in the *GHz* range.

Acknowledgments

The authors acknowledge partial financial support from Centers of excellence with BASAL/CONICYT financing, Grant FB0807, CEDENNA, CONICYT-ANILLO ACT 1410, Yachay Tech startup funds, UTA project 4733-17 and FONDECYT 1180905.

References

[1] C. Grebogi, E. Ott, S. Pelikan, J.A. Yorke, Physica D 13 (1984) 261–281.
[2] A. Bondenson, E. Ott, T.M. Antonsen Jr., Phys. Rev. Lett. 55 (1985) 2103–2106.
[3] F.J. Romeiras, E. Ott, Phys. Rev. A 35 (1987) 4404–4413.
[4] T. Kapitaniak, J. Wojewoda, Attractors of Quasi-Periodically Forced Systems, World Scientific, Singapore, 1994, and references therein.
[5] Y-C. Lai, Phys. Rev. E 53 (1996) 57–65.
[6] T. Yalçinkaya, Y.C. Lai, Phys. Rev. Lett. 77 (1996) 5039–5042.
[7] G. Keller, Fund. Math. 151 (1996) 139–148.
[8] U. Feudel, S. Kuznetsov, A. Pikovsky, Strange Nonchaotic Attractors, World Scientific, Singapore, 2006.
[9] B.R. Hunt, E. Ott, Phys. Rev. Lett. 87 (2001) 254101.
[10] J.W. Kim, S.Y. Kim, B. Hunt, E. Ott, Phys. Rev. E 67 (2003) 036211.
[11] W.L. Ditto, M.L. Spano, H.T. Savage, S.N. Rauseo, J. Heagy, E. Ott, Phys. Rev. Lett. 65 (1990) 533–536, and references therein.
[12] T. Zhou, F. Moss, A. Bulsara, Phys. Rev. A 45 (1992) 5394–5400.
[13] W.X. Ding, H. Deutsch, A. Dinklage, C. Wilke, Phys. Rev. E 55 (1997) 3769–3772.
[14] J.F. Lindner, V. Kohar, Behnam Kia, M. Hippke, J.G. Learned, W.L. Ditto, Phys. Rev. Lett. 114 (2015) 054101.
[15] K. Thamilmaran, D.V. Senthilkumar, A. Venkatesan, M. Lakshmanan, Phys. Rev. E 74 (2006) 036205.
[16] D.V. Senthilkumar, K. Srinivasan, K. Thamilmaran, M. Lakshmanan, Phys. Rev. E 78 (2008) 066211.
[17] A. Arulgnanam, A. Prasad, K. Thamilmaran, M. Daniel, Int. J. Bifurcation Chaos 25 (2015) 1530020.
[18] A. Arulgnanam, A. Prasad, K. Thamilmaran, M. Daniel, Chaos Solitons Fractals 75 (2015) 96–110.
[19] U. Feudel, J. Kurths, A.S. Pikovsky, Physica D 88 (1995) 176–186.
[20] T.E. Vadivasova, O.V. Sosnovtseva, A.G. Balanov, V.V. Astakhov, Phys. Rev E 61 (2000) 4618–4621.
[21] M.D. Shrimali, A. Prasad, R. Ramaswamy, U. Feudel, Phys. Rev. E 72 (2005) 036215.

[22] D. Laroze, D. Becerra-Alonso, J.A.C. Gallas, H. Pleiner, IEEE Trans. Magn. 11 (2012) 3567–3570.
[23] I.D. Mayergoyz, G. Bertotti, C. Serpico, Nonlinear Magnetization Dynamics in Nanosystems, Elsevier, Dordrecht, 2009.
[24] L.F. Alvarez, O. Pla, O. Chubykalo, Phys. Rev. B 61 (2000) 11613–11617.
[25] R.K. Smith, M. Grabowski, R.E. Camley, J. Magn. Magn. Mater. 322 (2010) 2127–2134.
[26] J. Bragard, H. Pleiner, O.J. Suarez, P. Vargas, J.A.C. Gallas, D. Laroze, Phys. Rev. E 84 (2011) 037202.
[27] D. Laroze, J. Bragard, O.J. Suarez, H. Pleiner, IEEE Trans. Magn. 47 (2011) 3032–3035.
[28] A. Pivano, V.O. Dolocan, Phys. Rev. B 93 (2016) 144410.
[29] A.M. Ferona, R.E. Camley, Phys. Rev. B 95 (2017) 104421.
[30] J. Slonczewski, J. Magn. Magn. Mater. 159 (1996) L1–L7.
[31] L. Berger, Phys. Rev. B 54 (1996) 9353–9358.
[32] I. Žutić, J. Fabian, S.D. Sarma, Rev. Mod. Phys. 76 (2004) 323–410.
[33] C. Chappert, A. Fert, F.N. Van Dau, Nat. Mater. 6 (2007) 813–823.
[34] J.A. Katine, E.E. Fullerton, J. Magn. Magn. Mater. 320 (2008) 1217–1226.
[35] M.N. Baibich, J.M. Broto, A. Fert, F. Nguyen Van Dau, F. Petroff, P. Eitenne, G. Creuzet, A. Friederich, J. Chazelas, Phys. Rev. Lett. 21 (1988) 2472–2475.
[36] G. Binasch, P. Grünberg, F. Saurenbach, W. Zinn, Phys. Rev. B 7 (1989) 4828–4830.
[37] D.C. Ralph, M.D. Stiles, J. Magn. Magn. Mater. 320 (2008) 1190–1216, and references therein.
[38] Phil Lakshmanan, Trans. R. Soc. A 369 (2011) 1280–1300.
[39] Z. Li, Y.C. Li, S. Zhang, Phys. Rev. B 74 (2006) 054417.
[40] Z. Yang, S. Zhang, Y.C. Li, Phys. Rev. Lett. 99 (2007) 134101.
[41] H.Z. Xu, X. Chen, J.M. Liu, J. App. Phys. 104 (2008) 093919.
[42] Y. Lan, Y.C. Li, Nonlinearity 21 (2008) 2801–2823.
[43] P.P. Horley, V.R. Vieira, P.M. Gorley, V.K. Dugaev, J. Berakdar, J. Barnaś, Phys. Rev. B 78 (2008) 054417.
[44] A. Slavin, V. Tiberkevich, IEEE Trans. Magn. 45 (2009) 1875–1918.
[45] S. Murugesh, M. Lakshmanan, Chaos 19 (2009) 043111.
[46] D. Gusakova, D. Houssameddine, U. Ebels, B. Dieny, L. Buda-Prejbeanu, M.C. Cyri, B. Delaët, Phys. Rev. B 79 (2009) 104406.
[47] M. d'Aquino, G. Di Fratta, C. Serpico, G. Bertotti, R. Bonin, I.D. Mayergoyz, J. Appl. Phys. 109 (2011) 07D349.
[48] B. Subash, V.K. Chandrasekar, M. Lakshmanan, EPL 102 (2013) 17010.
[49] B. Subash, V.K. Chandrasekar, M. Lakshmanan, Pramana -J. Phys. 84 (2015) 473–485.
[50] M.G. Clerc, S. Coulibaly, D. Laroze, A.O. Leon, A.S. Nuez, Phys. Rev. B 91 (2015) 224426.
[51] P.P. Horley, M.Ya. Kushnir, M. Morales-Meza, A. Sukhov, V. Rusyn, Phys. B 486 (2016) 60–63.
[52] D.V. Berkov, J. Miltat, J. Magn. Magn. Mater. 320 (2008) 1238–1259.
[53] S.I. Kiselev, J.C. Sankey, I.N. Krivorotov, N.C. Emley, R.J. Schoelkopf, R.A. Buhrman, D.C. Ralph, Nature 425 (2003) 380–383.
[54] S.I. Kiselev, J.C. Sankey, I.N. Krivorotov, N.C. Emley, M. Rinkoski, C. Perez, R.A. Buhrman, D.C. Ralph, Phys. Rev. Lett. 93 (2004) 036601.
[55] I.N. Krivorotov, N.C. Emley, R.A. Buhrman, D.C. Ralph, Phys. Rev. B 77 (2008) 054440.
[56] T. Nagasawa, H. Suto, K. Kudo, K. Mizushima, R. Sato, J. Appl. Phys. 109 (2011) 07C907.
[57] E. Beaurepaire, J.C. Merle, A. Daunois, J.Y. Bigot, Phys. Rev. Lett. 76 (1996) 4250–4253.
[58] B. Koopmans, M. van Kampen, J.T. Kohlhepp, W.J.M. de Jonge, Phys. Rev. Lett. 85 (2000) 844–847.
[59] J. Hohlfeld, E. Matthias, R. Knorren, K.H. Benemann, Phys. Rev. Lett. 78 (1997) 4861–4864.
[60] S. Kaka, S.E. Russek, Appl. Phys. Lett. 80 (2002) 2958–2960.
[61] S.-W. Lee, K.J. LEE, IEEE Trans. Magn. 46 (2010) 2349–2352.
[62] R.C. O' Handley, Modern Magnetic Materials: Principles and Applications, Wiley-Interscience, New York, 1999.
[63] B. Dieny, M. Chshiev, Rev. Mod. Phys. 89 (2017) 025008.
[64] J. Xiao, A. Zangwill, Phys. Rev. B 72 (2005) 014446.
[65] W. Kim, S.W. Lee, K. Lee, J. Phys. D: Appl. Phys. 44 (2011) 384001.
[66] A.O. Leon, D. Laroze, M.G. Clerc, A.M. Cabanas, Commun. Nonlinear Sci. Numer. Simul. 44 (2017) 404–413.
[67] S. Urazhdin, W.L. Lim, A. Higgins, Phys. Rev. B 78 (2008) 060405.
[68] S. Urazhdin, W.L. Lim, A. Higgins, Phys. Rev. B 80 (2009) 144411.
[69] C. Sanid, S. Murugesh, Phys. D: Appl. Phys. 47 (2014) 065005.
[70] S. Urazhdin, H. Kurt, W.P. Pratt, J. Bass Appl. Phys. Lett. 83 (2003) 114–116.
[71] M. Tsoi, A.G.M. Jansen, J. Bass, W.-C. Chiang, M. Seck, V. Tsoi, P. Wyder, Phys. Rev. Lett. 80 (1998) 4281–4284.
[72] M. Tsoi, V. Tsoi, J. Bass, A.G.M. Jansen, P. Wyder, Phys. Rev. Lett. 89 (2002) 246803.
[73] M. Tsoi, A.G.M. Jansen, J. Bass, W.-C. Chiang, V. Tsoi, P. Wyder, Nature 40 (2000) 46–48.
[74] A. Wolf, J.B. Swift, H.L. Swinney, J.A. Vastano, Physica D 16 (1985) 285–317.
[75] H. Gould, J. Tobochnik, An Introduction to Computer Simulation Methods: Applications to Physical Systems, second ed., Addison-Wesley, NY, 1996.
[76] A. Pikovsky, A. Politi, Lyapunov Exponents: A Tool to Explore Complex Dynamics, Cambridge University Press, Cambridge, 2016.
[77] F.J. Romeiras, A. Bondenson, E. Ott, T.M. Antonsen Jr., C. Grebogi, Physica D 26 (1987) 277–294.
[78] M. Ding, C. Grebogi, E. Ott, Phys. Rev. A 39 (1989) 2593–2598.
[79] M. Ding, J.A. Scott Kelso, Int. J. Bif. Chaos 4 (1994) 553–567.
[80] J.A.C. Gallas, Int. J. Bif. Chaos 20 (2010) 197–211.
[81] J.G. Freire, J.A.C. Gallas, Phys. Rev. E 82 (2010) 037202.
[82] L.M. Pérez, O.J. Suarez, D. Laroze, H.L. Mancini, Central Eur. J. Phys. 11 (2013) 1629–1637.
[83] O.V. Pylypovskyi, D.D. Sheka, V.P. Kravchuk, F.G. Mertens, Y. Gaididei, Phys. Rev. B 88 (2013) 014432.
[84] L.M. Pérez, J. Bragard, H.L. Mancini, J.A.C. Gallas, A.M. Cabanas, O.J. Suarez, D. Laroze, Netw. Heterog. Media 10 (2015) 209–221.
[85] T.V. Lyutyy, S.I. Denisov, A.Yu. Peletskyi, C. Binn, Phys. Rev. B 91 (2015) 054425.
[86] D. Urzagasti, D. Becerra-Alonso, L.M. Pérez, H.L. Mancini, D. Laroze, J. Low Temp. Phys. 181 (2015) 211–222.
[87] M.G. Phelps, K.L. Livesey, A.M. Ferona, R.E. Camley, Europhys. Lett. 109 (2015) 37007.
[88] O.J. Suarez, D. Laroze, J. Martínez-Mardones, D. Altbir, O. Chubykalo-Fesenko, Phys. Rev. B 95 (2017) 014404.
[89] J.A.C. Gallas, Phys. A 202 (1994) 196–223.
[90] A. Sack, J.G. Freire, E. Lindberg, T. Pöschel, J.A.C. Gallas, Sci. Rep. 3 (2013) 3350.
[91] R. Barrio, F. Blesa, S. Serrano, A. Shilnikov, Phys. Rev. E 84 (2011) 035201.